FULL PAPER

Dalton
www.rsc.org/dalton

The spin-states and spin-crossover behaviour of iron(II) complexes of 2,6-dipyrazol-1-ylpyrazine derivatives †

Jérôme Elhaïk,[a] Victoria A. Money,[b] Simon A. Barrett,[a] Colin A. Kilner,[a] Ivana Radosavljevic Evans[b] and Malcolm A. Halcrow*[a]

[a] *Department of Chemistry, University of Leeds, Woodhouse Lane, Leeds, UK LS2 9JT. E-mail: M.A.Halcrow@chem.leeds.ac.uk*

[b] *Department of Chemistry, University of Durham, South Road, Durham, UK DH1 3LE*

Received 22nd October 2002, Accepted 6th January 2003
First published as an Advance Article on the web 23rd April 2003

The syntheses of $[FeL_2]X_2$ (L = 2,6-dipyrazol-1-ylpyrazine [L^2H], 2,6-bis{3-methylpyrazol-1-yl}pyrazine [L^2Me], 2,6-bis{3,5-dimethylpyrazol-1-yl}pyrazine [L^2Me_2] or 2,6-bis{3-[2,4,6-trimethylphenyl]pyrazol-1-yl}pyrazine [L^2Mes]; $X^- = BF_4^-$ or ClO_4^-) are described. Solvent-free $[Fe(L^2H)_2][BF_4]_2$ and $[Fe(L^2H)_2][ClO_4]_2$ exhibit very similar abrupt spin-state transitions at 223 K and 208 K respectively, which show hysteresis loops of 3–5 K. Powder diffraction measurements afforded related, but not identical, unit cells for these two compounds, and imply that $[Fe(L^2H)_2][ClO_4]_2$ is isomorphous with $[Fe(L^1H)_2][BF_4]_2$ (L^1H = 2,6-dipyrazol-1-ylpyridine). The single crystalline solvate $[Fe(L^2H)_2][BF_4]_2 \cdot 3CH_3NO_2$ undergoes a similarly abrupt spin-state transition at 198 K. Polycrystalline $[Fe(L^2Me)_2][BF_4]_2$ and $[Fe(L^2Me)_2][ClO_4]_2$ are isomorphous with each other and also exhibit spin-state transitions at low temperature, although these are very different in form. In contrast, both salts of $[Fe(L^2Me_2)_2]^{2+}$ and $[Fe(L^2Mes)_2]^{2+}$ are fully low-spin at 295 K. Single crystal structures of $[Fe(L^2Me_2)_2][BF_4]_2 \cdot 0.5\{CH_3\}_2CO \cdot 0.1H_2O$ and $[Fe(L^2Mes)_2][BF_4]_2 \cdot 5CH_3NO_2$ show low-spin complex dications, and imply that $[Fe(L^2Me_2)_2][BF_4]_2$ is low-spin as a result of intra-ligand steric repulsions involving the pyrazole 5-methyl substituents. NMR and UV/vis data in MeCN and $MeNO_2$ show that the spin states of all four complex dications are similar in solution and the solid state except for $[Fe(L^2Me_2)_2]^{2+}$, which exists as a mixture of high- and low-spin species in these solvents.

Introduction

Although the phenomenon of spin-state transitions in d–d transition ion complexes has been known since the 1930's, there is continuing interest in the discovery of new spin-crossover compounds and their solid-state physics.[1,2] Much of this interest is driven by the potential technological applications for spin-crossover compounds, in display devices and for data storage.[3] To be useful in this regard, a spin-crossover material must be genuinely bistable. That is, its spin-state transition must show a hysteresis loop, so that within the hysteresis loop the compound can be either high-spin or low-spin, depending on its history. In addition, the transition should be abrupt, and occur as close to room temperature as possible. These properties depend on both the intra- and inter-molecular interactions within the solid compound,[1,2] and are difficult to engineer into a material. The most common structural motif in known spin-crossover compounds is of an octahedral Fe(II) centre with six N-donor ligands, and a large number of such compounds have been reported to date.

We have previously reported that $[Fe(L^1H)_2][BF_4]_2$ undergoes an abrupt spin-state transition at 261 K, exhibiting a small hysteresis loop.[4–6] The spin states of other complexes $[Fe(L^1R)_2]^{2+}$ that we have prepared vary in a predictable way depending on the inductive properties of the ligand 'R' substituents, when those substituents are sterically flat.[7,8] We therefore decided to introduce hydrogen-bonding functionality into the $[Fe(L^1R)_2]^{2+}$ framework, with the aim of increasing the cooperativity of any spin-state transitions we discovered. With this in mind, we report here the synthesis and characterisation of four complexes of type $[Fe(L^2R)_2]^{2+}$. The ligand L^2H and its Ag(I) complex have been reported previously,[9] as have some multi-dentate lanthanide chelators based on the L^2R framework.[10] We are aware of only a small number of other spin-crossover Fe(II) compounds containing pyrazine donors,[11–14] while three Fe(II) complexes of L^3 represent the only other known Fe(II) compounds with ligands containing both pyrazine and pyrazole functionalities.[15]

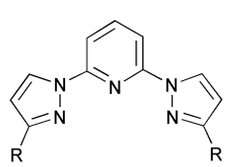

L^1R
(R = H, Pr^i, Ph, Mes)

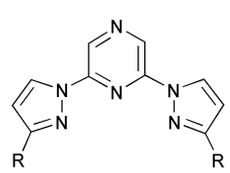

L^2R
(R = H, Me, Mes)

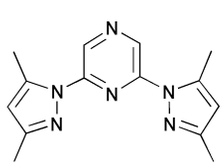

L^2Me_2

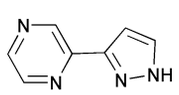

L^3

Results and discussion

The ligand L^2H was prepared by the published method.[9] The three new ligands in this study, L^2Me, L^2Me_2 and L^2Mes were synthesised by an analogous procedure employing the corresponding substituted pyrazole as starting material. The compounds $[Fe(L^2R)_2][BF_4]_2$ (R = H, **1[BF_4]$_2$**; R = Me, **2[BF_4]$_2$**; R = Me_2, **3[BF_4]$_2$**; R = Mes, **4[BF_4]$_2$**) and $[Fe(L^2R)_2][ClO_4]_2$ (R = H, **1[ClO_4]$_2$**; R = Me, **2[ClO_4]$_2$**; R = Me_2, **3[ClO_4]$_2$**; R = Mes, **4[ClO_4]$_2$**) can be prepared, by complexation of the relevant hydrated Fe(II) salt with 2 molar equivalents of L^2R in acetone. Once isolated, all these compounds are insoluble in acetone, but moderately soluble in MeCN or $MeNO_2$. For **4[BF_4]$_2$** and **4[ClO_4]$_2$** only, microanalysis consistently formulated these products as monohydrates (hereafter written as **4[BF_4]$_2$**$\cdot H_2O$ and **4[ClO_4]$_2$**$\cdot H_2O$). All of the other complexes were obtained as solvent free, anhydrous solids. We were unable

† Based on the presentation given at Dalton Discussion No. 5, 10–12th April 2003, Noordwijkerhout, The Netherlands.

DOI: 10.1039/b210368k

to prepare other hydrated crystals of salts of these compounds, since they undergo rapid hydrolysis in water or MeOH solution, precipitating free L^2R. A large number of co-crystallisations from aprotic solvents were also attempted of our $[Fe(L^2R)_2]^{2+}$ salts with aliphatic primary diamines or dialcohols, dihydroxybenzenes, or aliphatic or aromatic dicarboxylic acids. These were intended to exploit the hydrogen bond-acceptor capability of coordinated L^2R, to form infinite hydrogen-bonded solid lattices. However, all of these procedures yielded either additive-free $[Fe(L^2R)_2]X_2$ ($X^- = BF_4^-$, ClO_4^-), the pure additive, or an intractable mixture of species.

Solid state structures and magnetochemistry of $[Fe(L^2H)_2]^{2+}$ salts

Both **1[BF$_4$]$_2$** and **1[ClO$_4$]$_2$** are bright yellow microcrystalline powders, that show X_MT = 3.5 cm^3 mol^{-1} K at room-temperature. Both these observations are consistent with their being fully populated in a high-spin, $S = 2$ spin state.[16] Upon cooling, the samples undergo very similar abrupt spin-state transitions to a fully populated $S = 0$ low-spin form. For **1[BF$_4$]$_2$**, this transition is centred at 223 K and shows a hysteresis loop of 3 K, while for **1[ClO$_4$]$_2$**, the transition is centred at 206 K with a 5 K hysteresis loop (Fig. 1). These measurements were confirmed by DSC data, which showed one first-order transition for each material. For **1[BF$_4$]$_2$**, the DSC transition was centred at 224 K with a hysteresis width of 4 K, while for **1[ClO$_4$]$_2$** the transition was centred at 205 K with a 3 K hysteresis loop. Interestingly, the thermodynamic parameters for the transition in the two materials showed some differences. For **1[BF$_4$]$_2$**, ΔH = 29.2(1) kJ mol^{-1} and ΔS = 130.4(4) J mol^{-1} K^{-1}; while, for **1[ClO$_4$]$_2$** ΔH = 19.8(4) kJ mol^{-1} and ΔS = 97(2) J mol^{-1} K^{-1}. ΔH and ΔS for both of these compounds are somewhat greater than for $[Fe(L^1H)_2][BF_4]_2$,[4] however.

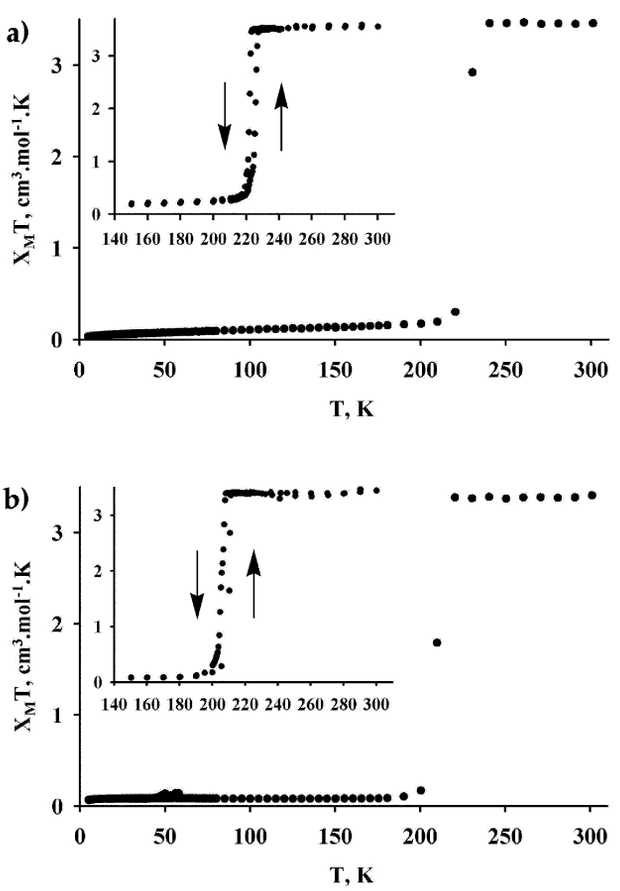

Fig. 1 Plots of X_MT *vs.* T for polycrystalline samples of: (a) **1[BF$_4$]$_2$**; and (b) **1[ClO$_4$]$_2$**. The inset graphs show the hysteresis loops associated with these two spin-state transitions.

Despite being centred at lower temperatures, the forms of the thermal spin-state transitions shown by **1[BF$_4$]$_2$** and **1[ClO$_4$]$_2$** in Fig. 1 are strikingly similar to that shown by $[Fe(L^1H)_2][BF_4]_2$,[4] which suggested to us that these three compounds might be isomorphous. Solvent-free single crystals of **1[BF$_4$]$_2$** and **1[ClO$_4$]$_2$** can be grown from acetone. Upon cooling on the diffractometer, these crystals undergo a sharp colour change from yellow to brown, at a temperature that is within 2 K of the spin-state transition temperature derived from powder magnetic measurements of these compounds (see above). Unfortunately, however, they diffract X-rays so poorly that we were unable to measure a unit cell from either compound. Therefore, we undertook powder diffraction measurements of these two solids at 295 K. Both compounds gave monoclinic P unit cells at this temperature, with the following parameters. For **1[BF$_4$]$_2$**: a = 11.886(2), b = 11.878(2), c = 19.093(3) Å, β = 92.291(9)° and V = 2693.4(8) Å^3. For **1[ClO$_4$]$_2$**: a = 8.694(1), b = 8.668(1), c = 19.993(3) Å, β = 90.517(1)° and V = 1506.5(1) Å^3. For comparison, single crystalline $[Fe(L^1H)_2][BF_4]_2$ has the following unit cell at 290 K: a = 8.4947(2), b = 8.5070(2), c = 19.0535(6) Å, β = 95.7050(18)° and V = 1370.07(6) Å^3.[4] The unit cell of **1[ClO$_4$]$_2$** is similar enough to that of $[Fe(L^1H)_2][BF_4]_2$ that the two compounds are almost certainly isomorphous. However, although the cell dimensions for **1[BF$_4$]$_2$** are superficially similar to these other two compounds ($a \approx b$, $c \approx 19$ Å, $\beta \approx 90°$), its unit cell volume is larger and corresponds approximately to $Z = 4$. These unit cells show that **1[BF$_4$]$_2$** and **1[ClO$_4$]$_2$** are likely to show similar, but not identical, packing arrangements in the solid that are closely related to that shown by $[Fe(L^2H)_2][BF_4]_2$.[4–6] Variable temperature powder diffraction measurements on these compounds are in progress, as are attempts to refine the structures of **1[BF$_4$]$_2$** and **1[ClO$_4$]$_2$** from their powder diffraction data. These will be reported separately.

Although useful single crystals of **1[BF$_4$]$_2$** and **1[ClO$_4$]$_2$** could not be grown, crystals of formula **1[BF$_4$]$_2$**·3CH$_3$NO$_2$ are good diffractors of X-rays. Interestingly, this compound is not isomorphous with the CH_3NO_2 solvate of $[Fe(L^1H)_2][BF_4]_2$.[5] The crystals are orange-yellow at room temperature, but undergo a sharp change to a dark brown colour upon cooling that is indicative of a spin-state transition. Variable temperature unit cell measurements established that this transition occurred abruptly at 198(1) K, and does not involve a crystallographic phase transition (Fig. 2). In cooling mode, the transition is characterised by a sharp increase of 1.18(10)° in the unit cell angle (in the setting $P2_1/n$), a 0.18(4) Å decrease in the unit cell dimension a and an increase of 0.064(13) Å in b; there is no significant discontinuity in the c dimension. These changes correspond to a decrease in the unit cell volume upon cooling across the transition of 30(4) Å^3, or 8(1) Å^3 per molecule which is much smaller than the volume change associated with spin-crossover in crystals of $[Fe(L^1H)_2][BF_4]_2$, of 18(3) Å^3 per molecule.[4–6] This presumably reflects the presence of additional solvent molecules in **1[BF$_4$]$_2$**·3CH$_3$NO$_2$, compared to the literature compound. Crystals of **1[BF$_4$]$_2$**·3CH$_3$NO$_2$ could be cycled across their transition several times, with only a small degradation in crystal quality.

Two X-ray datasets were collected from the same crystal of **1[BF$_4$]$_2$**·3CH$_3$NO$_2$ at 150 K and 300 K, which are temperatures at which the crystal should be fully low-spin and fully high-spin, respectively. At both temperatures, the complex dications show only small deviations from local D_{2d} symmetry (Fig. 3). The Fe–N bond lengths in **1[BF$_4$]$_2$**·3CH$_3$NO$_2$ at 150 K and 300 K are crystallographically indistinguishable from those in the low-spin and high-spin forms of $[Fe(L^1H)_2][BF_4]_2$,[4–6] respectively, and hence are consistent with the compound being in the expected, pure spin-state (Table 1). At both temperatures, all the BF_4^- and CH_3NO_2 moieties in the crystal are badly disordered. There are some differences in the disorder models refined at 150 K and 300 K, but it is uncertain how significant these changes are; or, if they are real, whether they result from

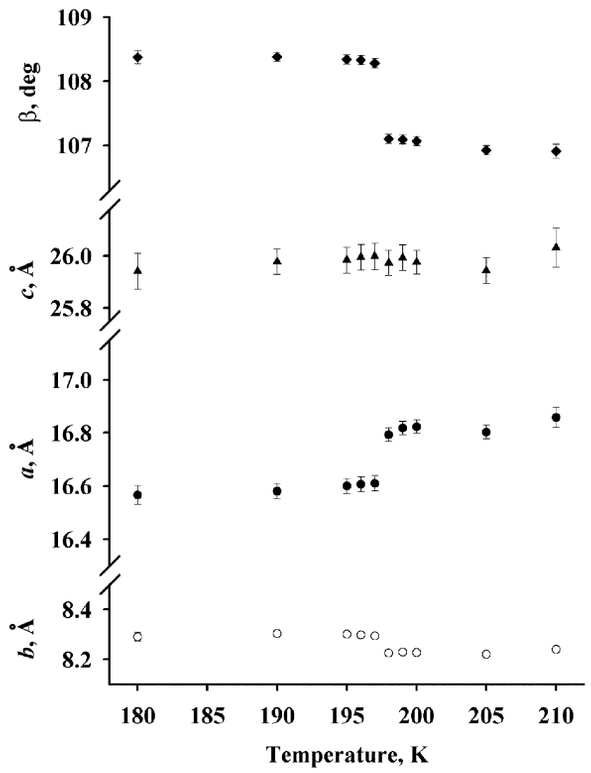

Fig. 2 Plot of the variation of the unit cell parameters of $\mathbf{1[BF_4]_2}\cdot 3CH_3NO_2$ with temperature.

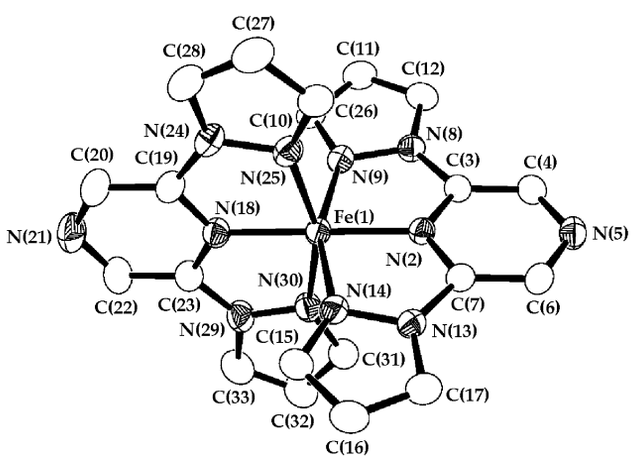

Fig. 3 View of the complex dication in the crystal structure of $[Fe(L^2H)_2][BF_4]_2\cdot 3CH_3NO_2$ ($\mathbf{1[BF_4]_2}\cdot 3CH_3NO_2$) at 150 K, showing the atom numbering scheme employed. For clarity, all H atoms have been omitted. Thermal ellipsoids are at the 50% probability level. The molecular structure of the complex dication in this crystal at 300 K is visually almost indistinguishable from that shown here, and uses an identical atom numbering scheme.

the spin state change, or simply from the effects of cooling the crystal. Hence, we have been unable to determine whether or not the abruptness of the spin-state change in the crystals is mediated by changes in the disorder regime of the crystal across the transition.[4,17]

Solid state structures and magnetochemistry of the other $[Fe(L^2R)_2]^{2+}$ complexes

Both of the salts $\mathbf{2[BF_4]_2}$ and $\mathbf{2[ClO_4]_2}$ are yellow at room temperature, showing that they are also high-spin under ambient conditions. Upon cooling they also undergo transitions to a low-spin state, although the shape of the X_MT *vs.* T curve is now very different for the two salts. The transition for $\mathbf{2[BF_4]_2}$ is very gradual, occurring over the approximate range of 130–280 K and being centred at 235 K (Fig. 4A). However, $\mathbf{2[ClO_4]_2}$

Table 1 Selected bond lengths (Å) and angles (°) for $[Fe(L^2H)_2][BF_4]_2\cdot 3CH_3NO_2$ ($\mathbf{1[BF_4]_2}\cdot 3CH_3NO_2$)

	150 K	300 K
Fe(1)–N(2)	1.896(3)	2.114(3)
Fe(1)–N(9)	1.982(3)	2.191(3)
Fe(1)–N(14)	1.981(3)	2.179(3)
Fe(1)–N(18)	1.891(3)	2.123(3)
Fe(1)–N(25)	1.998(3)	2.184(3)
Fe(1)–N(30)	1.978(3)	2.185(3)
N(2)–Fe(1)–N(9)	79.85(10)	73.21(11)
N(2)–Fe(1)–N(14)	79.53(10)	73.45(11)
N(2)–Fe(1)–N(18)	177.40(11)	173.18(11)
N(2)–Fe(1)–N(25)	102.60(10)	110.94(11)
N(2)–Fe(1)–N(30)	98.23(11)	102.97(11)
N(9)–Fe(1)–N(14)	159.37(11)	146.55(11)
N(9)–Fe(1)–N(18)	98.65(11)	101.54(11)
N(9)–Fe(1)–N(25)	91.18(10)	93.07(12)
N(9)–Fe(1)–N(30)	94.07(11)	97.97(12)
N(14)–Fe(1)–N(18)	101.98(11)	111.91(11)
N(14)–Fe(1)–N(25)	92.79(10)	96.25(12)
N(14)–Fe(1)–N(30)	89.38(11)	91.98(12)
N(18)–Fe(1)–N(25)	79.50(11)	73.27(12)
N(18)–Fe(1)–N(30)	79.73(11)	73.11(12)
N(25)–Fe(1)–N(30)	159.11(11)	146.07(12)

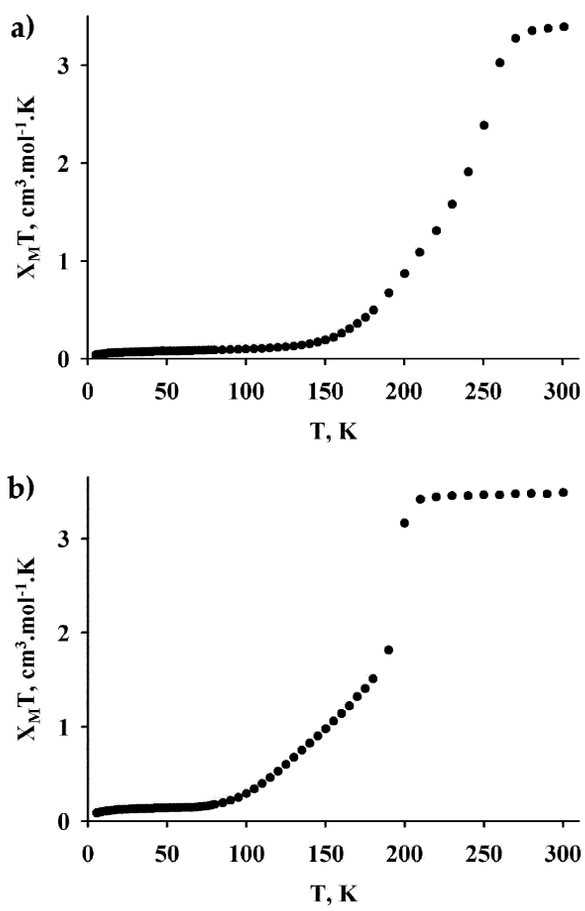

Fig. 4 Plots of X_MT *vs.* T for polycrystalline samples of: (a) $\mathbf{2[BF_4]_2}$ and (b) $\mathbf{2[ClO_4]_2}$.

shows a two-stage transition: an abrupt step at 196 K, that does not show detectable hysteresis; and a more gradual step centred at 133 K (Fig. 4B). The boundary between these two steps occurs when half of the Fe centres in the sample are low-spin, to within experimental error. From precedent, this behaviour could be interpreted in three ways. First, $\mathbf{2[ClO_4]_2}$ may contain two independent $[Fe(L^2Me)_2]^{2+}$ environments that undergo spin-state transitions at different temperatures.[18] Second, the

Table 2 Selected bond lengths (Å) and angles (°) for $[Fe(L^2Me_2)_2][BF_4]_2 \cdot 0.5\{CH_3\}_2CO \cdot 0.1H_2O$ (**3[BF$_4$]$_2$**·$0.5\{CH_3\}_2CO \cdot 0.1H_2O$)

Molecule 1		Molecule 2	
Fe(1)–N(2)	1.880(3)	Fe(42)–N(43)	1.885(3)
Fe(1)–N(9)	1.997(3)	Fe(42)–N(50)	1.967(3)
Fe(1)–N(16)	1.976(3)	Fe(42)–N(57)	1.989(3)
Fe(1)–N(22)	1.882(3)	Fe(42)–N(63)	1.884(3)
Fe(1)–N(29)	1.981(3)	Fe(42)–N(70)	1.979(3)
Fe(1)–N(36)	1.986(3)	Fe(42)–N(77)	1.984(3)
N(2)–Fe(1)–N(9)	80.30(12)	N(43)–Fe(42)–N(50)	80.21(12)
N(2)–Fe(1)–N(16)	80.12(12)	N(43)–Fe(42)–N(57)	80.33(12)
N(2)–Fe(1)–N(22)	176.10(12)	N(43)–Fe(42)–N(63)	179.50(14)
N(2)–Fe(1)–N(29)	101.53(13)	N(43)–Fe(42)–N(70)	99.30(13)
N(2)–Fe(1)–N(36)	98.59(12)	N(43)–Fe(42)–N(77)	100.21(13)
N(9)–Fe(1)–N(16)	160.41(12)	N(50)–Fe(42)–N(57)	160.54(12)
N(9)–Fe(1)–N(22)	96.27(12)	N(50)–Fe(42)–N(63)	100.14(12)
N(9)–Fe(1)–N(29)	92.24(12)	N(50)–Fe(42)–N(70)	90.60(12)
N(9)–Fe(1)–N(36)	93.67(12)	N(50)–Fe(42)–N(77)	93.37(13)
N(16)–Fe(1)–N(22)	103.32(12)	N(57)–Fe(42)–N(63)	99.32(12)
N(16)–Fe(1)–N(29)	91.27(12)	N(57)–Fe(42)–N(70)	92.45(12)
N(16)–Fe(1)–N(36)	89.63(12)	N(57)–Fe(42)–N(77)	90.15(13)
N(22)–Fe(1)–N(29)	80.37(13)	N(63)–Fe(42)–N(70)	80.35(13)
N(22)–Fe(1)–N(36)	79.70(12)	N(63)–Fe(42)–N(77)	80.13(13)
N(29)–Fe(1)–N(36)	159.71(12)	N(70)–Fe(42)–N(77)	160.47(12)

spin-state transition in this compound could occur concomitantly with a phase transition when the fraction of high-spin molecules in the solid ('γ') is 0.5, with the dynamics of the spin-crossover being different in the two phases.[19,20] Finally, a balance of inter- and intra-molecular forces within the solid may give rise to a local ordering of high- and low-spin molecules in the sample when $\gamma = 0.5$, without causing a crystallographic phase change.[21]

Single crystals of **2[BF$_4$]$_2$** and **2[ClO$_4$]$_2$** yield very similar unit cells at 150 K and at 300 K, all with 4/*m* Laue symmetry. At 150 K the parameters are as follows: for **2[BF$_4$]$_2$**, $a = 9.04(1)$, $c = 17.59(1)$ Å, $V = 1437.48(2)$ Å^3; and for **2[ClO$_4$]$_2$**, $a = 9.16(1)$, $c = 17.71(1)$ Å, $V = 1485.97(2)$ Å^3. Unfortunately, we were unable to solve crystallographic datasets obtained from either compound, and it is unclear whether or not the crystals were twinned. None-the-less, the unit cell volumes are consistent with the crystals being solvent-free (for $Z = 2$), and it seems clear that the two compounds are isomorphous. Hence, the very different spin-state transitions shown by the two compounds (Fig. 4) are intriguing. Unfortunately, in the absence of better crystallographic data we are unable to distinguish between the three potential origins of this behaviour listed in the previous paragraph.

In contrast, **3[BF$_4$]$_2$**, **4[BF$_4$]$_2$**·H$_2$O and their corresponding ClO_4^- salts are all dark brown in colour at room temperature. Magnetic measurements for all four compounds at 295 K showed X_MT <0.02 cm^3 mol^{-1} K, consistent with their being completely low spin under ambient conditions.[16] In order to understand the large difference in the magnetic properties between the complexes $[Fe(L^2Me)_2]^{2+}$ and $[Fe(L^2Me_2)_2]^{2+}$, a single crystal X-ray analysis was carried out on crystals of **3[BF$_4$]$_2$**·$0.5\{CH_3\}_2CO \cdot 0.1H_2O$ at 150 K. The asymmetric unit of the crystals contains two crystallographically independent complex dications, which show almost identical molecular structures with molecular symmetry close to D_{2d} (Fig. 5). The Fe–N bond lengths in this crystal structure (Table 2) are crystallographically indistinguishable from those in low-spin **1[BF$_4$]$_2$**·$3CH_3NO_2$ (Table 1) confirming that this compound is completely in a low-spin state at 150 K. Examination of a space-filling model shows that the 5-methyl groups on each pyrazole ring are in van-der-Waals contact with a 3{5}-H atom of the pyrazine ring. The relevant $H_3C \cdots H$ distances lie in the range 2.56–2.65 Å, compared to the sum of the Pauling radii of a H atom and a 'spherical' methyl group, of 3.2 Å.[22] Steric repulsion between these two groups should force the pyrazole N donors closer to the Fe ions, favouring a low-spin state. This presumably explains why **3[BF$_4$]$_2$** and **3[ClO$_4$]$_2$** are low-spin at room temperature.

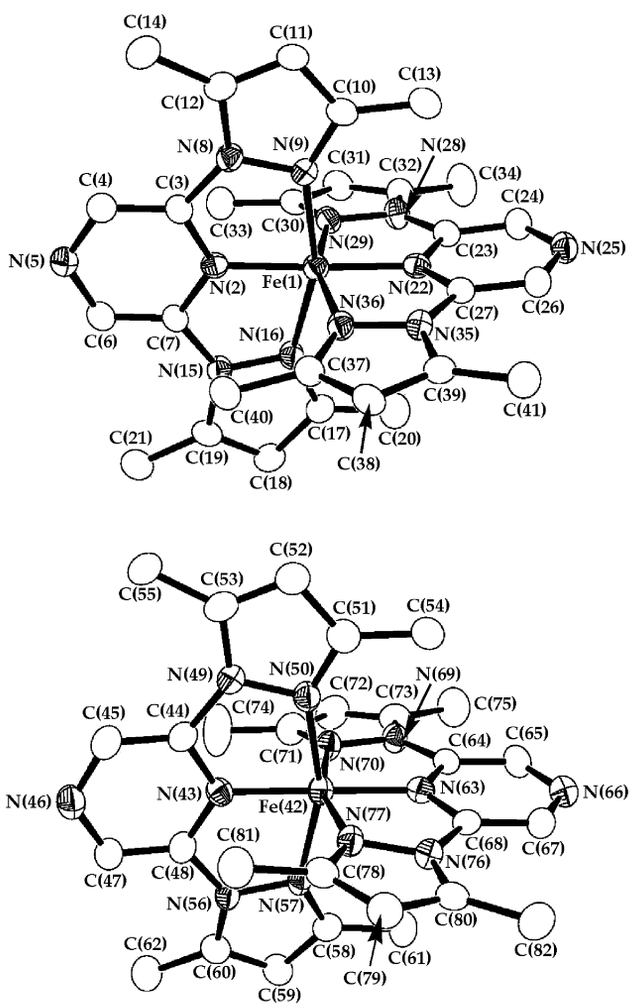

Fig. 5 Views of the crystallographically independent complex dications in the structure of $[Fe(L^2Me_2)_2][BF_4]_2 \cdot 0.5\{CH_3\}_2CO \cdot 0.1H_2O$ (**3[BF$_4$]$_2$**·$0.5\{CH_3\}_2CO \cdot 0.1H_2O$), showing the atom numbering scheme employed. For clarity, all H atoms have been omitted. Thermal ellipsoids are at the 50% probability level.

Table 3 Selected bond lengths (Å) and angles (°) for $[Fe(L^2Mes)_2][BF_4]_2 \cdot 5CH_3NO_2$ (**4[BF$_4$]$_2$**·$5CH_3NO_2$)

Fe(1)–N(2)	1.885(2)	Fe(1)–N(23)	2.009(2)
Fe(1)–N(9)	2.009(2)		
N(2)–Fe(1)–N(2′)	179.80(17)	N(9)–Fe(1)–N(9′)	87.80(13)
N(2)–Fe(1)–N(9)	80.01(9)	N(9)–Fe(1)–N(23)	160.09(9)
N(2)–Fe(1)–N(9′)	100.13(10)	N(9)–Fe(1)–N(23′)	95.79(9)
N(2)–Fe(1)–N(23)	80.08(9)	N(23)–Fe(1)–N23′)	87.49(13)
N(2)–Fe(1)–N(23′)	99.77(9)		

Primed atoms are related to unprimed atoms by the relation $y, x, -z$.

A crystal structure was also achieved on crystals of **4[BF$_4$]$_2$**·$5CH_3NO_2$, to probe the apparent lattice water found in this compound. The structure shows a fully low-spin Fe(II) centre, with crystallographic C_2 symmetry and approximate D_{2d} symmetry (Fig. 6, Table 3). The Fe–N bond lengths in this structure are up to 0.042(4) Å longer than for low-spin **1[BF$_4$]$_2$**·$3CH_3NO_2$ or **3[BF$_4$]$_2$**, but are similar to those in $[Fe(L^1Mes)_2][PF_6]_2$.[7] Importantly, even though dried material from the same solvent analyses as **4[BF$_4$]$_2$**·H_2O, there is no trace of lattice water in the solvated crystals analysed here. This shows that the water content of the dried material does not play an intrinsic role in its structure, but is simply atmospheric moisture that has partially replaced the nitromethane content of the freshly prepared crystals upon exposure to air. We have observed this previously in salts of $[M(L^1Mes)_2]^{2+}$ (M = Fe,[7] Co,[23] Ni,[23] Cu,[24] Zn[25]), which always form solvated single crystals from CH_3NO_2 or CH_3CN and are very difficult to obtain as solvent-free solids. Hence, it seems unlikely that the water content in powdered **4[BF$_4$]$_2$**·H_2O interacts specifically with this complex's non-coordinated pyrazine N donors.

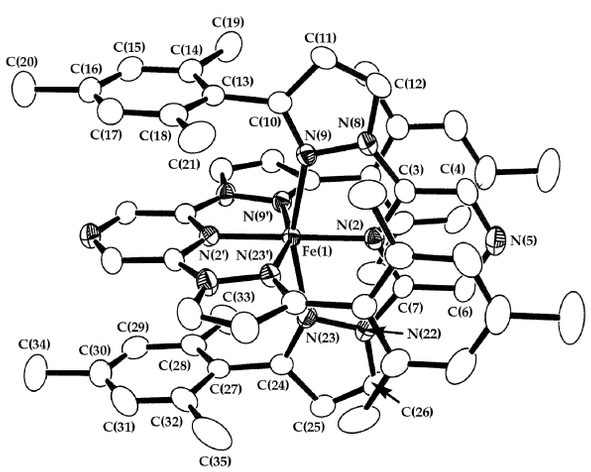

Fig. 6 View of the complex dication in the crystal structure of $[Fe(L^2Mes)_2][BF_4]_2 \cdot 5CH_3NO_2$ (**4[BF$_4$]$_2$**·$5CH_3NO_2$), showing the atom numbering scheme employed. For clarity, all H atoms have been omitted. Thermal ellipsoids are at the 50% probability level. Primed atoms are related to unprimed atoms by the relation $y, x, -z$.

Solution measurements

All solution studies were carried out using the BF_4^- salts of the complexes. The ^{1}H NMR spectra of all these complexes show a single C_2 or *m*-symmetric L^2R environment, consistent with the D_{2d}-symmetric molecular structures shown by, or anticipated for, these compounds. The spectra of **1[BF$_4$]$_2$**, **2[BF$_4$]$_2$** and **3[BF$_4$]$_2$** in CD_3CN at 295 K were all broadened and strongly contact shifted, consistent with these compounds being at least partly high-spin in solution. In contrast, the spectrum of **4[BF$_4$]$_2$**·H_2O is well resolved, and lies completely within the diamagnetic region of the spectrum. This demonstrates that this complex is completely low-spin in solution. These data are consistent with the solid-state properties of **1[BF$_4$]$_2$**, **2[BF$_4$]$_2$** and **4[BF$_4$]$_2$**·H_2O (see above). However, the contact-shifted spectrum of **3[BF$_4$]$_2$** was unexpected, since this compound is fully low-spin in the solid at this temperature. ^{1}H NMR spectra obtained in CD_3NO_2 showed the same number of peaks as in CD_3CN, at chemical shifts that were identical for each compound to within ±2 ppm for the paramagnetic spectra, or ±0.2 ppm for the diamagnetic spectra. However, for **1[BF$_4$]$_2$** only the spectrum in CD_3CN was substantially broader than in CD_3NO_2. This could indicate the presence of solvent-promoted ligand exchange for this compound in CD_3CN, which would be consistent with the sensitivity of the $[Fe(L^2R)_2]^{2+}$ complexes to hydrolysis mentioned above.

Low temperature solution-phase magnetic data were not measured for **1[BF$_4$]$_2$** and **2[BF$_4$]$_2$**, owing to their very poor solubility in solvents that have freezing points near their solid state spin-state transitions, such as $\{CD_3\}_2CO$. However, the magnetic moment of **3[BF$_4$]$_2$** was measured in CD_3NO_2 between 253 K and 333 K, in order to gain further insight into its unexpected NMR and UV/vis behaviour (see below). Under these conditions X_MT rose continuously from 0.5(1) cm^3 mol^{-1} K at 253 K to 1.0(1) cm^3 mol^{-1} K at 333 K. A spin-state transition in solution would yield an S-shaped X_MT *vs.* T curve, and would normally be complete over a temperature range of *ca.* 150 K.[5,26] So, the extremely slow monotonic rise of X_MT with increasing temperature shown by **3[BF$_4$]$_2$** is unlikely to correspond to a single Fe(II) centre in a spin equilibrium. Rather, it implies a solution sample containing a mixture of high- and low-spin Fe(II) complex species in rapid temperature-dependent chemical exchange. This is further evidence for solution lability of another of our $[Fe(L^2R)_2]^{2+}$ centres.

The UV/vis/NIR spectra of the compounds in CH_3CN and CH_3NO_2 at 295 K are listed in the Experimental section. Very similar spectra were obtained in the visible and near-UV ranges in both solvents for each compound, which confirm the conclusions drawn from the NMR studies. Hence, **1[BF$_4$]$_2$** and **2[BF$_4$]$_2$** show spectra arising from a pure high-spin Fe(II) chromophore, being characterised by two overlapping d–d absorptions centred near 9.3 and 11.8 × 10^3 cm^{-1}, both with $\varepsilon_{max} \approx 10$ M^{-1} cm^{-1};[27] and, a weak metal-to-ligand charge transfer (MLCT) band near 23.5 × 10^3 cm^{-1} (sh, $\varepsilon \approx 250$ M^{-1} cm^{-1}). Compound **4[BF$_4$]$_2$**·H_2O, in contrast, exhibits spectra typical of a low-spin Fe(II) centre,[27] that is dominated by a much stronger MLCT envelope centred at 22.4 × 10^3 cm^{-1} ($\varepsilon_{max} \approx 3{,}200$ M^{-1} cm^{-1}). However, the spectrum of **3[BF$_4$]$_2$** shows both a d–d absorption characteristic of a high-spin compound at 12.0 × 10^3 cm^{-1} (11.4); and, a strong MLCT band at 21.2 × 10^3 cm^{-1} (3,000) that is suggestive of a low-spin Fe(II) centre. This is consistent with the NMR data mentioned above, which show that **3[BF$_4$]$_2$** exists as a mixture of high-spin and low-spin compounds under these conditions.

Conclusion

The compounds in this study represent a continuation of our investigations of Fe(II) complexes of pyrazine-containing chelates. Unlike our earlier system $[Fe(L^3)_3]^{2+}$,[15] salts of $[Fe(L^2H)_2]^{2+}$ and $[Fe(L^2Me)_2]^{2+}$ undergo spin-state transitions at moderately low temperatures in the solid state and in solution. Comparison of these data with our earlier results[4–6] shows that substitution of the pyridine rings in $[Fe(L^1R)_2]^{2+}$ by pyrazine rings in $[Fe(L^2R)_2]^{2+}$ results in only a small lowering of the spin-crossover temperature, by *ca.* 50 K. This small effect of introducing an additional heteroatom into $[Fe(L^2R)_2]^{2+}$ compared to $[Fe(L^1R)_2]^{2+}$ is also reflected in the low-spin character of $[Fe(L^2Mes)_2]^{2+}$. Since we have previously shown that $[Fe(L^1Mes)_2]^{2+}$ is low-spin,[7] and because $[Fe(L^2H)_2]^{2+}$ shows a lower spin-crossover temperature than $[Fe(L^1H)_2]^{2+}$, we had hoped that substitution of a pyrazine ring for the pyridine ring in the ligand framework may lower the ligand field at Fe sufficiently for $[Fe(L^2Mes)_2]^{2+}$ to show a spin-state transition at or below room temperature. Clearly, this is not the case. It

is also of interest that **1[BF$_4$]$_2$**, **1[BF$_4$]$_2$**·3CH$_3$NO$_2$, **1[ClO$_4$]$_2$**, **2[BF$_4$]$_2$** and **2[ClO$_4$]$_2$** all undergo spin-state transitions at broadly similar temperatures, with $T_{½}$ = 196–235 K. Studies on related tridentate ligand systems have implied that $T_{½}$ for [Fe(L^{2}Me)$_2$]$^{2+}$ should be lower for than [Fe(L^{2}H)$_2$]$^{2+}$, because of the inductive effect of the ligand methyl substituents;[28] or, that it should be higher than for [Fe(L^{2}H)$_2$]$^{2+}$, owing to steric repulsions involving these methyl groups.[29] Clearly, these effects balance out in our system, so that these two complex dications undergo spin-state transitions at very similar temperatures.

The apparent solution lability of **1[BF$_4$]$_2$** and **3[BF$_4$]$_2$**, and the sensitivity of all of our compounds to hydrolysis in protic solvents, contrasts with [Fe(L^{1}R)$_2$]$^{2+}$ (R = H, Pr^i, Ph, Mes), which exhibit static structures by NMR[5,7] and which are much more chemically robust. Presumably, the increased lability of [Fe(L^{2}R)$_2$]$^{2+}$ reflects the lower basicity of the pyrazine donor in L^{2}R compared to the pyridine donor in L^{1}R,[30] combined with the relatively poor basicity of the pyrazole donors in both ligands.[31]

It is interesting that, although we have synthesised and crystallised our compounds in air, using non-predried solvents, few of the crystalline or powder solids we have isolated contain lattice water, or any other protic additives that might hydrogen bond to the non-coordinated pyrazine N-donors. In addition, while the salts of [Fe(L^{2}Mes)$_2$]$^{2+}$ that we prepared appear to contain lattice water by microanalysis, this is not present in single crystals of **4[BF$_4$]$_2$** grown from the same solvent. The apparent reluctance of [Fe(L^{2}R)$_2$]$^{2+}$ to engage in hydrogen bonding contrasts with the known Fe(II) complexes of L^3, all of which contain extensive hydrogen bonding to the L^3 pyrazine acceptors.[15] We suggest that the incorporation of a second electron-withdrawing pyrazole substituent into the L^{2}R ring may reduce the basicity of the non-coordinated L^{2}R N-atom to such an extent that it is only a poor hydrogen-bond acceptor. Future work will investigate the synthesis of pyrazine-based ligands containing other donor functions with more favourable inductive properties, in order to ameliorate this problem.

Experimental

Unless stated otherwise, all manipulations were performed in air using commercial grade solvents, except that pre-dried dmf was purchased from Aldrich and stored under N$_2$. 2,6-Dipyrazol-1-ylpyrazine (L^{2}H)[9] and 3{5}-(2,4,6-trimethylphenyl)pyrazole[32] were prepared by the literature procedures. All other reagents were used as supplied.

Synthesis of 2,6-bis(3-methylpyrazol-1-yl)pyrazine (L^{2}Me)

A deoxygenated solution of 3{5}-methylpyrazole (2.0 g, 2.4 × 10^{-2} mol) in dry dmf (250 cm^3) was added to solid KH (1.0 g, 2.5 × 10^{-2} mol) under N$_2$, and the resultant suspension stirred at 50 °C for 20 minutes. 2,6-Dichloropyrazine (1.8 g, 1.2 × 10^{-2} mol) was then added, and the mixture stirred at 90 °C for 16 h. After cooling, a large excess of cold water was added to the mixture, yielding a white solid which was collected, washed with water and dried over P$_2$O$_5$. This crude solid contained both L^{2}Me, and its regioisomer 2-(3-methylpyrazolyl)-6-(5-methylpyrazolyl)pyrazine in approximately 4 : 1 molar ratio by ^{1}H NMR. Recrystallisation of the mixture from acetone allowed the isolation of pure L^{2}Me as a white solid, albeit with substantial solubility losses. Yield 1.2 g, 40%. Found: C, 59.7; H, 5.0; N, 35.2; Calcd. for C$_{12}$H$_{12}$N$_6$: C, 60.0; H, 5.0; N, 35.0%. Mp 164–166 °C. EI mass spectrum: *m*/*z* 240 [M]$^+$. NMR spectra (CDCl$_3$, 295 K): ^{1}H; δ 9.08 (s, 2H, Py *H*$^{3/5}$), 8.36 (d, 2.0 Hz, 2H, Pz *H*^{5}), 6.31 (d, 2.0 Hz, 2H, Pz *H*^{4}), 2.39 (s, 6H, C*H*$_3$) ppm. ^{13}C; δ 153.1 (Pz *C*$^{2/6}$), 144.9 (Pz *C*^{3}), 130.6, 128.0 (Py *C*$^{3/5}$ + Pz *C*^{5}), 109.1 (Pz *C*^{4}), 13.8 (*C*H$_3$) ppm.

Synthesis of 2,6-bis(3,5-dimethylpyrazol-1-yl)pyrazine (L^{2}Me$_2$)

Method as for L^{2}Me, using 3,5-dimethylpyrazole (2.3 g, 2.4 × 10^{-2} mol). The freshly precipitated white solid product was analytically pure after drying over P$_2$O$_5$, and was not purified further. Yield 4.6 g, 70%. Found: C, 62.8; H, 6.2; N, 31.3; Calcd. for C$_{14}$H$_{16}$N$_6$: C, 62.7; H, 6.0; N, 31.3%. Mp 167–169 °C. EI mass spectrum: *m*/*z* 268 [M]$^+$. NMR spectra (CDCl$_3$, 295 K): ^{1}H; δ 9.05 (s, 2H, Py *H*$^{3/5}$), 6.05 (d, 2.0 Hz, 2H, Pz *H*^{4}), 2.61 (s, 6H, 5-C*H*$_3$), 2.32 (s, 6H, 3-C*H*$_3$) ppm. ^{13}C; δ 151.3 (Py *C*$^{2/6}$), 146.4 (Pz *C*^{3}), 141.6 (Pz *C*^{5}), 134.5 (Py *C*$^{3/5}$), 109.9 (Pz *C*^{4}), 14.1, 13.6 (2 × *C*H$_3$) ppm.

Synthesis of 2,6-bis(3-{2,4,6-trimethylphenyl}pyrazol-1-yl)-pyrazine (L^{2}Mes)

Method as for L^{2}Me, using 3{5}-(2,4,6-trimethylphenyl)-pyrazole (4.2 g, 2.4 × 10^{-2} mol). The freshly precipitated white solid product solid contained L^{2}Mes, and its regioisomer 2-(3-{2,4,6-trimethylphenyl}pyrazolyl)-6-(5-{2,4,6-trimethylphenyl}-pyrazolyl)pyrazine in approximately 9 : 1 molar ratio by ^{1}H NMR. Recrystallisation of the mixture from acetone allowed the isolation of pure L^{2}Mes as a white solid, albeit with substantial solubility losses. Yield 1.6 g, 31%. Found: C, 74.2; H, 6.2; N, 18.7; Calcd. for C$_{28}$H$_{28}$N$_6$: C, 75.0; H, 6.3; N, 18.7%. Mp 189–191 °C. EI mass spectrum: *m*/*z* 448 [M]$^+$. NMR spectra (CDCl$_3$, 293 K): ^{1}H; δ 9.20 (s, 2H, Py *H*$^{3/5}$), 8.60 (d, 2.8 Hz, 2H, Pz *H*^{5}), 6.98 (s, 4H, Ph *H*$^{3/5}$), 6.54 (d, 2.8 Hz, 2H, Pz *H*^{4}), 2.34 (s, 6H, 4–C*H*$_3$), 2.20 (s, 12H, 2,6–C*H*$_3$) ppm. ^{13}C; δ 154.9 (Py *C*$^{2/6}$), 145.1 (Pz *C*^{3}), 138.2 (Ph *C*^{4}), 137.3 (Ph *C*$^{2/6}$), 131.4 (Py *C*$^{3/5}$), 129.7 (Ph *C*^{1}), 128.4 (Ph *C*$^{3/5}$), 127.7 (Pz *C*^{5}), 110.4 (Pz *C*^{4}), 21.1 (4–*C*H$_3$), 20.5 (2,6–*C*H$_3$) ppm.

Syntheses of the complexes

The syntheses of all of these complexes followed the same basic procedure, as described here for [Fe(L^{2}H)$_2$][BF$_4$]$_2$ (**1[BF$_4$]$_2$**). A solution of Fe[BF$_4$]$_2$·6H$_2$O (0.24 g, 7.2 × 10^{-4} mol) and L^{2}H (0.30 g, 1.4 × 10^{-3} mol) in acetone (50 cm^3) was stirred at room temperature for 15 min. The resultant yellow solution was filtered and concentrated to *ca.* 1/3 its original volume, whereupon a yellow precipitate formed. Following overnight storage at −30 °C, the product was filtered off and washed sequentially with cold MeOH and Et$_2$O. Small amounts of this product can be recrystallised from the same solvent mixture, yielding solvent-free microcrystals. Similar reactions using equivalent quantities of the appropriate L^{2}R ligand and Fe[ClO$_4$]$_2$·6H$_2$O, yielded the other complexes in this study. Yields ranged from 59–86%. [**CAUTION**: while we have experienced no difficulty in handling the ClO$_4^-$ salts in this study, metal–organic perchlorates are potentially explosive and should be handled with due care in small quantities.]

For [Fe(L^{2}H)$_2$][BF$_4$]$_2$ (**1[BF$_4$]$_2$**): found C, 36.8; H, 2.8; N, 25.5. Calcd. For C$_{20}$H$_{16}$B$_2$F$_8$FeN$_{12}$: C, 36.7; H, 2.5; N, 25.7%. ES mass spectrum: *m*/*z* 499 [^{56}FeF(L^{2}H)$_2$]$^+$, 240 [^{56}Fe(L^{2}H)$_2$]$^{2+}$. ^{1}H NMR spectrum (CD$_3$CN, 295 K): δ 55.2 (8H), 33.2, 11.0 (both 4H) (Py *H*$^{3/5}$ + Pz *H*^{3}–*H*^{5}) ppm. UV/vis spectrum (MeCN, 295 K): ν_{max}, 10^3 cm^{-1} (ε_{max}, M^{-1}.cm^{-1}) 9.2 (sh), 11.4 (9.5), 23.5 (sh), 30.7 (37,300), 37.3 (22,500), 40.9 (49,328), 41.5 (sh), 46.5 (22,300). UV/vis spectrum (MeNO$_2$, 295 K): ν_{max}, 10^3 cm^{-1} (ε_{max}, M^{-1}.cm^{-1}) 9.2 (sh), 11.8 (12.0).

For [Fe(L^{2}H)$_2$][ClO$_4$]$_2$ (**1[ClO$_4$]$_2$**): found C, 35.4; H, 2.4; N, 24.8. Calcd. For C$_{20}$H$_{16}$Cl$_2$FeN$_{12}$O$_8$: C, 35.4; H, 2.4; N, 24.7%. ES mass spectrum: *m*/*z* 579 [^{56}Fe^{35}ClO$_4$(L^{2}H)$_2$]$^+$, 367 [^{56}Fe^{35}ClO$_4$(L^{2}H)]$^+$, 240 [^{56}Fe(L^{2}H)$_2$]$^{2+}$.

For [Fe(L^{2}Me)$_2$][BF$_4$]$_2$ (**2[BF$_4$]$_2$**): found C, 40.6; H, 3.4; N, 23.6. Calcd. For C$_{24}$H$_{24}$B$_2$F$_8$FeN$_{12}$: C, 40.6; H, 3.4; N, 23.7%. ES mass spectrum: *m*/*z* 315 [^{56}FeF(L^{2}Me)]$^+$, 268 [^{56}Fe(L^2-Me)$_2$]$^{2+}$. ^{1}H NMR spectrum (CD$_3$CN, 295 K): δ 68.6, 68.4, 37.4 (all 4H, Py *H*$^{3/5}$ + Pz *H*^{4}, *H*^{5}), 7.3 (12H, C*H*$_3$) ppm. UV/vis spectrum (MeCN, 295 K): ν_{max}, 10^3 cm^{-1} (ε_{max}, M^{-1}.cm^{-1})

Table 4 Experimental details for the single crystal structure determinations in this study

	$1[BF_4]_2\cdot 3CH_3NO_2$		$3[BF_4]_2\cdot 0.5\{CH_3\}_2CO\cdot 0.1H_2O$	$4[BF_4]_2\cdot 5CH_3NO_2$
Formula	$C_{23}H_{25}B_2F_8FeN_{15}O_6$	$C_{23}H_{25}B_2F_8FeN_{15}O_6$	$C_{29.5}H_{35.2}B_2F_8FeN_{12}O_{0.6}$	$C_{61}H_{71}B_2F_8FeN_{17}O_{10}$
M_r	837.05	837.05	796.96	1431.82
Crystal class	Monoclinic	Monoclinic	Monoclinic	Hexagonal
Space group	$P2_1/n$	$P2_1/n$	$P2_1/c$	$P3_12_1$
a/Å	16.5404(2)	16.9138(2)	11.3306(1)	15.1838(1)
b/Å	8.2833(1)	8.3045(1)	15.2392(2)	–
c/Å	25.8237(4)	26.3119(4)	40.5559(5)	24.9779(2)
β/°	108.2104(6)	107.4285(4)	92.8371(6)	–
V/Å^3	3360.89(8)	3526.13(8)	6994.17(14)	4987.09(6)
Z	4	4	8	3
μ(Mo-K$_\alpha$)/mm^{-1}	0.558	0.531	0.518	0.320
T/K	150(2)	300(2)	150(2)	150(2)
Measured reflections	23212	30653	62394	89750
Independent reflections	7664	6902	15966	7623
R_{int}	0.047	0.083	0.128	0.157
$R(F)^a$	0.064	0.079	0.061	0.057
$wR(F^2)^b$	0.196	0.248	0.162	0.160
Flack parameter	–	–	–	0.004(19)

^{a} $R = \Sigma[|F_o| - |F_c|] / \Sigma|F_o|$. ^{b} $wR = [\Sigma w(F_o^2 - F_c^2) / \Sigma wF_o^4]^{½}$.

9.4 (sh), 11.8 (9.9), 23.6 (sh), 30.3 (44,600), 36.6 (27,700), 40.2 (56,400), 45.0 (sh). UV/vis spectrum ($MeNO_2$, 295 K): ν_{max}, 10^3 cm^{-1} (ε_{max}, M^{-1}.cm^{-1}) 9.7 (sh), 11.8 (11.3).

For $[Fe(L^2Me)_2][ClO_4]_2$ (**2[ClO$_4$]$_2$**): found C, 39.1; H, 3.2; N, 22.8. Calcd. For $C_{24}H_{24}Cl_2FeN_{12}O_8$: C, 39.2; H, 3.3; N, 22.9%. ES mass spectrum: m/z 635 $[^{56}Fe^{35}ClO_4(L^2Me)_2]^+$, 395 $[^{56}Fe^{35}ClO_4(L^2Me)]^+$, 269 $[^{56}Fe(L^2Me)_2]^{2+}$.

For $[Fe(L^2Me_2)_2][BF_4]_2$ (**3[BF$_4$]$_2$**): found C, 44.0; H, 4.4; N, 21.8. Calcd. For $C_{28}H_{32}B_2F_8FeN_{12}$: C, 43.9; H, 4.2; N, 21.8%. ES mass spectrum: m/z 611 $[^{56}FeF(L^2Me_2)_2]^+$, 296 $[^{56}Fe(L^2Me_2)_2]^{2+}$. ^{1}H NMR spectrum ($CD_3CN$, 295 K): δ 39.3, 38.3 (both 4H, Py $H^{3/5}$ + Pz H^4), 14.6, 4.3 (both 12H, CH_3) ppm. UV/vis spectrum (MeCN, 295 K): ν_{max}, 10^3 cm^{-1} (ε_{max}, M^{-1}.cm^{-1}) 12.0 (11.4), 18.5 (sh), 21.2 (3,000), 22.4 (sh), 24.8 (sh), 30.7 (32,500), 37.1 (sh), 40.2 (45,300). UV/vis spectrum ($MeNO_2$, 295 K): ν_{max}, 10^3 cm^{-1} (ε_{max}, M^{-1}.cm^{-1}) 11.8 (11.0), 21.0 (3,000), 22.3 (sh).

For $[Fe(L^2Me_2)_2][ClO_4]_2$ (**3[ClO$_4$]$_2$**): found C, 42.2; H, 4.0; N, 21.4. Calcd. For $C_{28}H_{32}Cl_2FeN_{12}O_8$: C, 42.2; H, 4.1; N, 21.2%. ES mass spectrum: m/z 691 $[^{56}Fe^{35}ClO_4(L^2Me_2)_2]^+$, 296 $[^{56}Fe(L^2Me_2)_2]^{2+}$.

For $[Fe(L^2Mes)_2][BF_4]_2\cdot H_2O$ (**4[BF$_4$]$_2$**·H$_2$O): found C, 58.9; H, 5.1; N, 14.8. Calcd. For $C_{56}H_{56}B_2F_8FeN_{12}\cdot.H_2O$ C, 58.8; H, 5.1; N, 14.7%. ES mass spectrum: m/z 476 $[^{56}Fe(L^2Mes)_2]^{2+}$. ^{1}H NMR spectrum (CD_3CN, 295 K): δ 9.08 (d, 3.0 Hz, 4H, Pz H^5), 9.01 (s, 4H, Py $H^{3/5}$), 6.73 (s, 8H, Ph $H^{3/5}$), 6.61 (d, 3.0 Hz, 4H, Pz H^4), 2.36 (s, 12H, 4-CH_3), 0.96 (s, 24H, 2,6-CH_3) ppm. UV/vis spectrum (MeCN, 295 K): ν_{max}, 10^3 cm^{-1} (ε_{max}, M^{-1}.cm^{-1}) 11.3 (3.2), 15.2 (sh), 22.4 (3,200), 29.7 (31,500), 35.8 (sh), 38.9 (48,300), 45.0 (sh). UV/vis spectrum ($MeNO_2$, 295 K): ν_{max}, 10^3 cm^{-1} (ε_{max}, M^{-1}.cm^{-1}) 11.3 (3.9), 16.3 (sh), 22.3 (3,400), 23.5 (sh).

For $[Fe(L^2Mes)_2][ClO_4]_2\cdot H_2O$ (**4[ClO$_4$]$_2$**·H$_2$O): found C, 57.5; H, 4.9; N, 14.6. Calcd. For $C_{56}H_{56}Cl_2FeN_{12}O_8.H_2O$: C, 57.5; H, 5.0; N, 14.4%. ES mass spectrum: m/z 1051 $[^{56}Fe^{35}ClO_4(L^2Mes)_2]^+$, 476 $[^{56}Fe(L^2Mes)_2]^{2+}$.

Single crystal X-ray structure determinations

Single crystals of X-ray quality of **1[BF$_4$]$_2$**·3CH$_3$NO$_2$, and **3[BF$_4$]$_2$**·0.5{CH$_3$}$_2$CO·0.1H$_2$O and **4[BF$_4$]$_2$**·5CH$_3$NO$_2$ were grown by diffusion of diethyl ether vapour into solutions of the complexes in the appropriate solvents. Experimental details for these structure determinations are given in Table 4. All structures were solved by direct methods (SHELXS 97[33]) and refined by full matrix least-squares on F^2 (SHELXL 97[34]).

CCDC reference numbers 195908–195910 and 199771.

See http://www.rsc.org/suppdata/dt/b2/b210368k/ for crystallographic data in CIF or other electronic format.

X-Ray structure determination of $[Fe(L^2H)_2][BF_4]_2\cdot 3CH_3NO_2$ ($1[BF_4]_2\cdot 3CH_3NO_2$). Two datasets were collected from the same crystal of this compound, at 300 and 150 K. At both temperatures, both BF_4^- anions and all three CH_3NO_2 molecules suffered from disorder. Each of these disordered moieties was modelled over two or three different orientations, although the precise model used varied slightly between the two refinements. The following refined restraints were applied to the final models: at 150 K, B–F = 1.39(2), non-bonded F ··· F = 2.27(2), C–N = 1.47(2), N–O = 1.22(2) and non-bonded O ··· O = 2.11(2) Å; at 300 K, B–F = 1.39(2), non-bonded F ··· F = 2.27(2), C–N = 1.47(2), N–O = 1.21(2) and non-bonded O ··· O = 2.10(2) Å. All crystallographically ordered non-H atoms were refined anisotropically. All H atoms were placed in calculated positions and refined using a riding model except for the disordered solvent methyl H groups, which were fixed in idealised geometries and whose torsions were not refined.

X-Ray structure determination of $[Fe(L^2Me_2)_2][BF_4]_2\cdot 0.5\{CH_3\}_2CO\cdot 0.1H_2O$ ($3[BF_4]_2\cdot 0.5\{CH_3\}_2CO\cdot 0.1H_2O$). The asymmetric unit of this crystal contains two complex dications, four BF_4^- anions, one molecule of acetone, and one weakly scattering feature not bonded to any other residue that was modelled as a molecule of water with occupancy 0.2. Three of the four BF_4^- anions was disordered, each being modelled over three different orientations. All disordered B–F bonds were restrained to 1.39(2) Å, and non-bonded F ··· F distances within a given disorder orientation to 2.27(2) Å. All non-H atoms with occupancy ≥0.5 were refined anisotropically. All H atoms were placed in calculated positions and refined using a riding model except for the H atoms attached to the partial water molecule, which were not included in the final model. The putative partial water molecule is not positioned to be a hydrogen-bond donor to any of the pyrazine N atoms.

X-Ray structure determination of $[Fe(L^2Mes)_2][BF_4]_2\cdot 5CH_3NO_2$ ($4[BF_4]_2\cdot 5CH_3NO_2$). The asymmetric unit contains: half a complex dication, with Fe(1) lying on the crystallographic C_2 axis y, x, $-z$; one BF_4^- anion lying on a general position; two CH_3NO_2 molecules lying on general positions; and, half a CH_3NO_2 molecule lying across the C_2 axis $-x$, $-x+y$, $\frac{1}{3}-z$. The BF_4^- anion is disordered, and was modelled over three equally occupied orientations. All of the CH_3NO_2 molecules were also disordered. One of these was modelled over

2 equally occupied orientations, while another was modelled using three partial CH_3NO_2 molecules with a 0.50 : 0.25 : 0.25 occupany ratio. The solvent molecule lying across the C_2 axis was modelled using one orientation bisected by the two-fold axis with occupancy 0.5; and, a second partial molecule on a general position near the C_2 axis, with occupancy 0.25. The following refined restraints were applied to the final model: B–F = 1.39(2), non-bonded F ··· F = 2.27(2), C–N = 1.43(2), N–O = 1.24(2) and non-bonded O ··· O = 2.16(2) and C ··· O 2.29(2) Å. All crystallographically ordered non-H atoms were refined anisotropically. All H atoms were placed in calculated positions and refined using a riding model except for the disordered solvent methyl H groups, which were fixed in idealised geometries and whose torsions were not refined.

Other measurements

Infra-red spectra were obtained as Nujol mulls pressed between NaCl windows between 600 and 4,000 cm^{-1} using a Nicolet Avatar 360 spectrophotometer. UV/vis spectra were obtained with a Perkin-Elmer Lambda 900 spectrophotometer operating between 3300 and 200 nm, in 1 cm quartz cells. All NMR spectra were run on a Bruker DPX250 spectrometer, operating at 250.1 (^{1}H) and 62.9 (^{13}C) MHz. Electron impact mass spectra were performed on a Kratos MS50 spectrometer, while electrospray mass spectra were obtained on a Micromass LCT TOF spectrometer, employing a MeOH matrix. CHN microanalyses were performed by the University of Leeds School of Chemistry microanalytical service. Melting points are uncorrected. Differential scanning calorimetry data were obtained using a Perkin-Elmer Pyris calorimeter, with a temperature ramp of 5 K min^{-1}.

Room-temperature magnetic data were measured using a Sherwood Scientific magnetic susceptibility balance. Variable temperature magnetic susceptibility measurements were obtained in the solid state using a Quantum Design SQUID magnetometer operating at 1000 G. Scans between 5 and 300 K were run using a continuous temperature ramp, while for hysteresis measurements, the sample was poised at each temperature for 1 minute before measurement. Diamagnetic corrections for the sample and the sample holder were applied to the data. Magnetic susceptibility measurements in solution were obtained by Evan's method[35] using a Bruker DRX500 spectrometer operating at 500.13 MHz. A diamagnetic correction for the sample, and a correction for variation of the density of the CD_3NO_2 solvent with temperature,[36] were applied to these data. Diamagnetic corrections were estimated from Pascal's constants.[16]

Acknowledgements

The authors gratefully thank Dr H. J. Blythe (University of Sheffield) for the variable temperature susceptibility measurements. The Royal Society (M. A. H.), the EPSRC (J. E., V. A. M.) and the University of Leeds are acknowledged for financial support.

References

1 P. Gütlich, A. Hauser and H. Spiering, *Angew. Chem., Int. Ed. Engl.*, 1994, **33**, 2024.
2 P. Gütlich, Y. Garcia and H. A. Goodwin, *Chem. Soc. Rev.*, 2000, **29**, 419.
3 O. Kahn, *Science*, 1998, **179**, 44.
4 J. M. Holland, J. A. McAllister, Z. Lu, C. A. Kilner, M. Thornton-Pett and M. A. Halcrow, *Chem. Commun.*, 2001, 577.
5 J. M. Holland, J. A. McAllister, C. A. Kilner, M. Thornton-Pett, A. J. Bridgeman and M. A. Halcrow, *J. Chem. Soc., Dalton Trans.*, 2002, 548.
6 V. A. Money, I. Radosavljevic Evans, M. A. Halcrow, A. E. Goeta and J. A. K. Howard, *Chem. Commun.*, 2003, 158.
7 J. M. Holland, S. A. Barrett, C. A. Kilner and M. A. Halcrow, *Inorg. Chem. Commun.*, 2002, **5**, 328.
8 J. Elhaïk, C. A. Kilner and M. A. Halcrow, unpublished work.
9 M. Loï, M. W. Hosseini, A. Jouaiti, A. De Cian and J. Fischer, *Eur. J. Inorg. Chem.*, 1999, 1981.
10 J. C. Rodriguez-Ubis, R. Sedano, G. Barroso, O. Juanes and E. Brunet, *Helv. Chim. Acta*, 1997, **80**, 86.
11 J. A. Real, M. C. Muñoz, E. Andrés, T. Granier and B. Gallois, *Inorg. Chem.*, 1994, **33**, 3587.
12 B. J. Childs, D. C. Craig, K. A. Russ, M. L. Scudder and H. A. Goodwin, *Aust. J. Chem.*, 1994, **47**, 891.
13 B. J. Childs, J. M. Cadogan, D. C. Craig, M. L. Scudder and H. A. Goodwin, *Aust. J. Chem.*, 1997, **50**, 129.
14 V. Niel, J. M. Martinez-Agudo, M. C. Muñoz, A. B. Gaspar and J. A. Real, *Inorg. Chem.*, 2001, **40**, 3838.
15 R. J. Smithson, C. A. Kilner, A. R. Brough and M. A. Halcrow, *Polyhedron*, in the press.
16 C. J. O'Connor, *Prog. Inorg. Chem.*, 1982, **29**, 203.
17 E. N. Maslen, C. L. Raston and A. H. White, *J. Chem. Soc., Dalton Trans.*, 1974, 1803.
18 P. Poganiuch, S. Descurtins and P. Gütlich, *J. Am. Chem. Soc.*, 1990, **112**, 3270; R. Hinek, H. Spiering, D. Schollmeyer, P. Gütlich and A. Hauser, *Chem. Eur. J.*, 1996, **2**, 1427; Y. Garcia, O. Kahn, L. Rabardel, B. Chansou, L. Salmon and J.P. Tuchagues, *Inorg. Chem.*, 1999, **38**, 4663.
19 D. Boinnard, A. Bousseskou, A. Dworkin, J. M. Savariault, F. Varret and J. P. Tuchagues, *Inorg. Chem.*, 1994, **33**, 271.
20 D. L. Reger, C. A. Little, A. L. Rheingold, M. Lam, L. M. Liable-Sands, B. Rhagitan, T. Concolino, A. Mohan, G. J. Long, V. Briois and F. Grandjean, *Inorg. Chem.*, 2001, **40**, 1508; D. L. Reger, C. A. Little, V. G. Young jr. and M. Pink, *Inorg. Chem.*, 2001, **40**, 2870; D. L. Reger, C. A. Little, M. D. Smith and G. J. Long, *Inorg. Chem.*, 2002, **41**, 4453.
21 R. Jakobi, H. Spiering and P. Gütlich, *J. Phys. Chem. Solids*, 1992, **53**, 267; J. A. Real, H. Bolvin, A. Bousseskou, A. Dworkin, O. Kahn, F. Varret and J. Zarembowitch, *J. Am. Chem. Soc.*, 1992, **114**, 4650.
22 L. Pauling, *The Nature of the Chemical Bond*, Cornell University Press, Ithaca, New York, 3rd edn., 1960, pp. 257–264.
23 J. M. Holland, C. A. Kilner, M. Thornton-Pett and M. A. Halcrow, *Polyhedron*, 2001, **20**, 2829.
24 N. K. Solanki, E. J. L. McInnes, F. E. Mabbs, S. Radojevic, M. McPartlin, N. Feeder, J. E. Davies and M. A. Halcrow, *Angew. Chem., Int. Ed.*, 1998, **37**, 2221; N. K. Solanki, M. A. Leech, E. J. L. McInnes, J. P. Zhao, F. E. Mabbs, N. Feeder, J. A. K. Howard, J. E. Davies, J. M. Rawson and M. A. Halcrow, *J. Chem. Soc., Dalton Trans.*, 2001, 2083.
25 M. A. Halcrow, C. A. Kilner and M. Thornton-Pett, *Acta Crystallogr., Sect. C.*, 2000, **56**, 1425.
26 See *e.g.* H. L. Chum, J. A. Vanin and M. I. D. Holanda, *Inorg. Chem.*, 1982, **21**, 1146; L. L. Martin, K. S. Hagen, A. Hauser, R. L. Martin and A. M. Sargeson, *J. Chem. Soc., Chem. Commun.*, 1988, 1313; D. W. Blakesley, S. C. Payne and K. S. Hagen, *Inorg. Chem.*, 2000, **39**, 1979; S. G. Telfer, B. Bocquet and A. F. Williams, *Inorg. Chem.*, 2001, **40**, 4818.
27 A. B. P. Lever, *Inorganic Electronic Spectroscopy*, Elsevier, Amsterdam, 2nd edn., 1984, pp. 458–470.
28 K. H. Sugiyarto, D. C. Craig, A. D. Rae and H. A. Goodwin, *Aust. J. Chem.*, 1993, **46**, 1269.
29 A. T. Baker and H. A. Goodwin, *Aust. J. Chem.*, 1986, **39**, 209; A. T. Baker, P. Singh and V. Vignevich, *Aust. J. Chem.*, 1991, **34**, 1041.
30 A. Albert, R. Goldacre and J. Phillips, *J. Chem. Soc.*, 1948, 2240.
31 J. Elguero, E. Gonzalez and R. Jacquier, *Bull. Soc. Chim. Fr.*, 1968, 5009.
32 A. L. Rheingold, C. B. White and S. Trofimenko, *Inorg. Chem.*, 1993, **32**, 3471.
33 G. M. Sheldrick, *Acta Crystallogr., Sect. A.*, 1990, **46**, 467.
34 G. M. Sheldrick, SHELXL 97, Program for the Refinement of Crystal Structures, University of Göttingen, Germany, 1997.
35 E. M. Schubert, *J. Chem. Educ.*, 1992, **69**, 62.
36 P. Oakley, *J. Chem. Soc.*, 1924, 1194.